

Friction Stir Processing of a High Entropy Alloy Al_{0.1}CoCrFeNi

N. KUMAR,¹ M. KOMARASAMY,¹ P. NELATURU,¹ Z. TANG,²
P.K. LIAW,² and R.S. MISHRA^{1,3}

1.—Department of Materials Science and Engineering, Center for Friction Stir Processing, University of North Texas, Denton, TX 76203, USA. 2.—Department of Materials Science and Engineering, The University of Tennessee, Knoxville, TN 37996, USA. 3.—e-mail: Rajiv.Mishra@unt.edu

High entropy alloys are a new class of metallic materials with a potential for use in structural applications. However, most of the studies have focused on microhardness and compressive strength measurements for mechanical properties determination. This study presents the tensile deformation behavior of a single-phase, face-centered cubic Al_{0.1}CoCrFeNi high entropy alloy (HEA). Friction stir processing was carried out to refine the grain size. Scanning electron microscopy and electron backscatter diffraction were carried out for microstructural examination. The grain size of the alloy was on the order of millimeters in the as-received condition. The average grain size after friction stir processing of the alloy was 14 ± 10 micrometers. The mechanical properties were determined through microhardness measurement and mini-tensile tests. The friction stir processed alloy showed a total elongation of $\sim 75\%$ for the mini-tensile sample used and yield strength of 315 MPa. It is an exceptional combination of strength and ductility. Friction stress was determined to be 174 MPa and the Hall–Petch coefficient was $371 \text{ MPa} (\mu\text{m})^{1/2}$. Such a high value of Hall–Petch coefficient suggests that grain boundary strengthening can be a very effective strengthening mechanism for the HEA Al_{0.1}CoCrFeNi.

INTRODUCTION

Although alloy design based on one predominant element has been the norm, the start of the twenty-first century saw a great departure from conventional alloying principles. The new alloying principle has led to the emergence of a new class of compositionally concentrated alloys, which are known as high entropy alloys (HEAs). These alloys are also called multiprincipal elements alloy and multicomponent alloys. The HEA name has been attributed to this class of material due to their high configurational entropy compared with the entropy of fusion of many conventional metals.^{1,2} In a very conservative approach, Yeh et al.³ showed that it was possible to develop ~ 8000 new alloys based on the HEA design principle. If one goes by the estimate of Miracle et al.⁴ then the number of equimolar alloys can be as high as 127,000. Although the paradigm based on high entropy alloys is still in its infancy, the scientific and technological explorations are expected to lead to a “new science” and products superior in performance than those based on conventional alloys.

The alloys developed based on this new paradigm have shown many material properties either at par or exceeding that exhibited by conventional alloys. Figure 1 shows a tetrahedron for the design of engineering components that involves the plastic deformation of alloys. It includes the fatigue-limited design, yield strength-limited design, toughness-limited design, and creep-limited design. Note that the best property in each category is exhibited by HEAs.^{1,5–7} This observation based on the initial set of results is really encouraging and shows the future potential of HEAs as structural materials.

Based on the initial potential of HEAs, it is important to further study mechanical properties to understand the deformation behavior of HEAs in different microstructural states. To this end, a host of researchers are globally engaged in investigating several mechanical properties including uniaxial compressive and tensile properties.^{1,2,4,8,9}

In the current work, friction stir processing (FSP) was used for the microstructural modification of a high entropy alloy. FSP is a derivative of the friction stir welding technique, which was developed at The

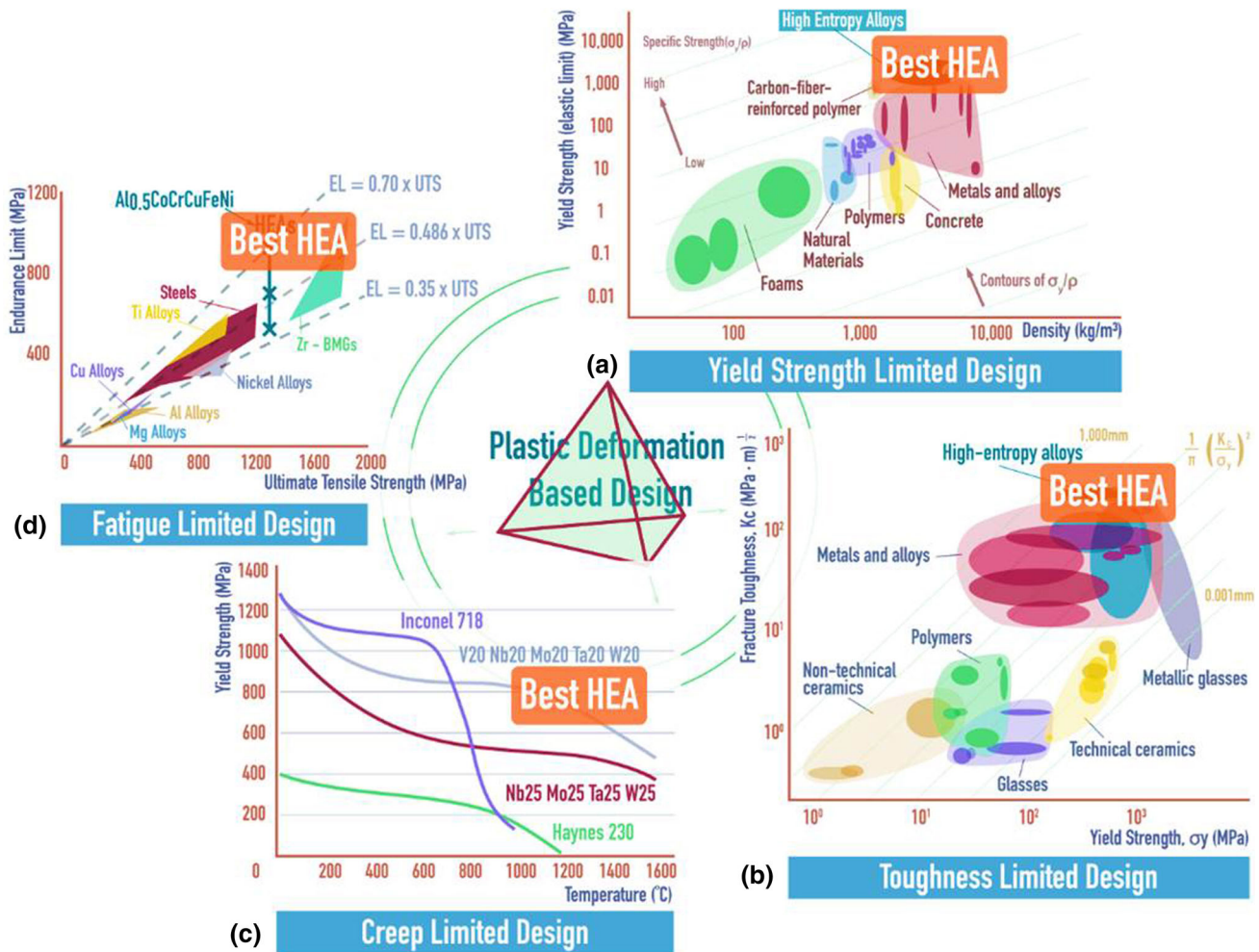


Fig. 1. Plastic deformation-based design tetrahedron showing superior properties of high entropy alloys among conventional alloys (a) Yield strength limited design (b) Toughness limited design, (c) Creep limited design, and (d) Fatigue limited design. The data were taken from Refs. 1 and 5–7.

Welding Institute, United Kingdom, in 1991.¹⁰ The concept of FSP as a generic microstructural modification tool was introduced by Mishra et al.¹¹ Different friction stir process attributes have led to the development of various friction stir technologies.¹² A series of recent publications ascertain the role FSP plays in the development of fine-grained, equiaxed, randomly oriented grains, and low dislocation density microstructures.^{13–15} The current work has been undertaken to understand the effect of microstructural refinement using FSP on plastic deformation behavior of a high entropy alloy. The friction stress and Hall–Petch coefficient parameters present in the Hall–Petch equation have been calculated in this work for the HEA studied.

EXPERIMENTAL

A single-phase, face-centered-cubic (fcc) $\text{Al}_{0.1}\text{CoCrFeNi}$ HEA (nominal composition, at.%: Al—2.44 and rest 24.4 each) was used for FSP. The HEA was prepared at The University of Tennessee,

Knoxville. The steps involved in the making of the HEA were as follows: (I) vacuum-induction melting (a $127 \times 305 \times 19 \text{ mm}^3$ cast plate), (II) hot isostatic pressing (HIP) by argon at a pressure of 103 MPa and a temperature of 1204°C for 4 h, and (III) cooling to 343°C in 3 h followed by cooling down to 191°C in 1 h and then removal from the vessel. A polycrystalline cubic boron nitride (PCBN) tool having a convex, scrolled shoulder and conical pin with spiral feature on it was used for FSP of the HEA. The tool rotation rate, tool traverse speed, tool tilt, and plunge depth were 600 rpm, $\sim 1 \text{ ipm}$ (25 mm/min), 2.5°, and 5.0 mm, respectively. FSP was carried out in the ambient condition, and the backing plate was made of tool steel. Figure 2 includes the picture of the tool used during FSP.

The FEI Quanta ESEM (FEI Company, Hillsboro, OR) was used to take the macroscopic image of the transverse cross-section of the alloy in the friction stir processed condition. EBSD was employed for the microstructural examination of the as-received and friction stir processed alloy. The EBSD (using a TSL

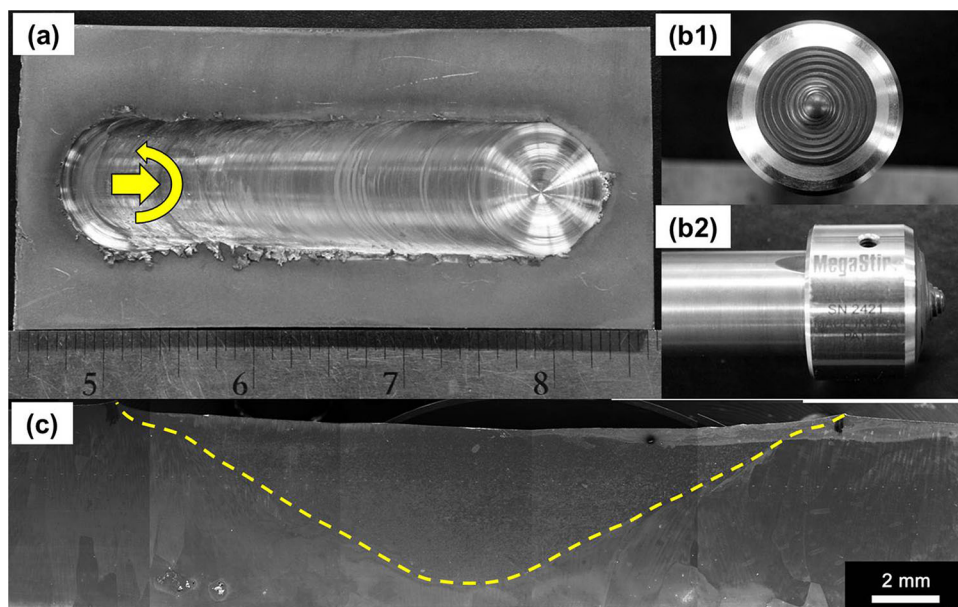


Fig. 2. (a) Top surface of the plate showing the friction stir processed zone, (b1 and b2) PCBN tool used for the processing, and (c) transverse cross-section showing the macroscopic appearance of the nugget with respect to the base material.

EBSD system interfaced with FESEM Nova 200) was carried out on the transverse cross-section at the center of the nugget. The following parameters were used during EBSD data acquisition: voltage = 20 kV, current = 2.4 nA, working distance of ~ 10 – 11 mm for both as-received and friction stir processed conditions, scan step of $5 \mu\text{m}$ for as-received and $1 \mu\text{m}$ for friction stir processed conditions.

Vickers microhardness measurements of the alloy in as-received and friction stir processed conditions were carried out using 500-g load with 10-s loading cycle. For the measurement of tensile properties, uniaxial tensile testing was done for the alloy in both conditions using a custom-built tensile tester. The gage length, width, and thickness of tensile samples were ~ 2.0 mm, ~ 1.1 mm, and ~ 0.6 mm, respectively. The gage of the mini-tensile sample was oriented along the transverse to the friction stir processing direction. Tensile testing was carried out at an initial strain rate of 10^{-3} s^{-1} and at room temperature. Final polishing was done using $1\text{-}\mu\text{m}$ grit size polycrystalline diamond suspension for all samples before tensile testing. In each condition, two samples were tested for the repeatability of the test result.

RESULTS AND DISCUSSIONS

Figure 2a shows a macroscopic view of the top surface of the friction stir processed region. The sense of tool rotation and travel directions are also marked. A very smooth and shiny surface of the material with little flash should be noted here in the processed zone. Note that materials like ferrous and titanium alloys need protective atmosphere, such as the presence of argon gas during FSP to avoid sur-

face oxidation. In this study, no protective atmosphere was provided and visually it appeared that no significant oxidation occurred during FSP. As mentioned, Fig. 2b1, b2 show different perspectives of the PCBN tool used in FSP of the alloy. In Fig. 2c, the transverse cross-section of the plate is shown. The broken line identifies boundaries between the nugget and the rest of the plate. The region below the broken line shows very large grains, whereas an entirely different appearance of the grains (indistinguishable at this magnification) in the nugget should be noted here.

Figure 3a shows the EBSD map of the alloy in the as-received condition. It shows grains on the order of millimeters. The same observations regarding the grain size were made based on the region lying below the dotted line in Fig. 2c. The grain structure after FSP is shown in Fig. 3b, which as expected is significantly finer than that in the as-received condition. The high-angle grain boundaries (HAGBs) are shown by black lines in Fig. 3b. The yellow lines represent annealing twins and $\Sigma 3$ special boundaries. The average grain size was determined to be $\sim 14 \pm 10 \mu\text{m}$ with an HAGB cut-off angle of 15° . An uncorrelated misorientation distribution analysis (not shown here) revealed a Mackenzie distribution indicative of a random distribution of the grains in the friction stir processed microstructure.¹⁶

The microhardness measurement results are shown in Fig. 4a. The microhardness value of the as-received material is represented by the dash-dotted horizontal line in this figure. The hardness of the as-received material was $132 \pm 3 \text{ HV}0.5$. The hardness values of the nugget region shows a significant improvement in hardness after FSP with an average hardness value of $181 \pm 5 \text{ HV}0.5$ in the

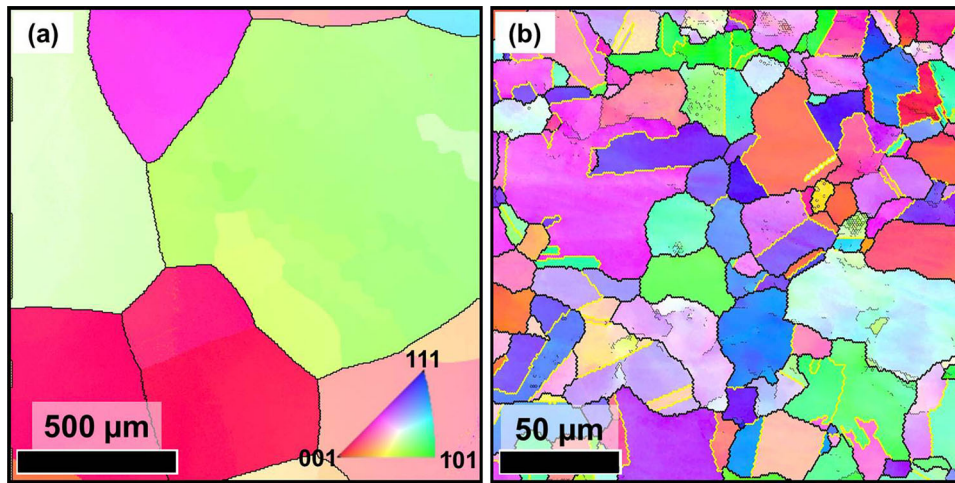


Fig. 3. EBSD map of (a) as-received and (b) friction stir processed samples. The color associated with each grain represents a particular crystallographic axis perpendicular to the plane of the paper, and its index can be assessed from the inverse pole figure triangle embedded in (a).

nugget region and an improvement of ~ 50 HV0.5 over the as-received alloy.

The stress–strain curves (engineering and true) are presented in Fig. 4b. The average yield strength (YS) of the alloy in the as-received condition was 150 ± 1 MPa. Note that the gage length, width, and thickness of the tensile samples were ~ 2.0 mm, ~ 1.1 mm, and ~ 0.6 mm, respectively. Given that the grains are very coarse in the as-received alloy, the gage section of the tensile sample is not expected to contain more than a few grains. In addition to this trend, based on the processing history of the alloy, the dislocation density is also expected to be negligible. Hence, the YS of the as-received alloy is mainly due to the contribution coming from the lattice friction stress in this single-phase fcc alloy. The average YS of the friction stir processed alloy was 315 ± 4 MPa. Note that after FSP, the average grain size was 14 ± 10 μm . Hence, the gage section of the tensile sample contained a sufficient number of grains for YS, in this condition, to be representative of a polycrystalline behavior. Therefore, in the FSP condition, the YS of the material is composed of the lattice friction stress and grain boundary strengthening. In general, the nugget microstructure shows very low dislocation density after FSP.¹² FSP is a high-temperature thermomechanical processing technique. When a given volume of the material is left on the trailing side of the tool, it remains in the wake of the thermal field, which causes recovery of the deformed material volume resulting in low dislocation density. Hence, it was assumed that the contribution of dislocation strengthening to the YS of the alloy in the friction stir processed condition was limited and can be neglected.

In low-stacking-fault metallic materials, a three-stage work hardening has been reported in the literature.¹⁷ It is schematically shown in the inset of Fig. 4c, bounded within gray rectangular regions, and each stage is labeled with the letters A, B, and C.

Figures 4c, d include the variation of strain-hardening rates as functions of true strain and true stress, respectively, for the as-received and friction stir processed alloys. Given the presence of very limited grains in the gage section of the as-received alloy, the work-hardening behavior is dependent on the orientation of each crystal with respect to the loading axis (tensile axis).¹⁸ Hence, although included in Fig. 4c, d, the work-hardening behavior of the alloy in the as-received condition will not be discussed in this study. Before the discussion of the work-hardening behavior of the friction stir processed alloy, a general consideration of the stage B is important. In the inset, it is shown with a positive slope to emphasize the discontinuity. In general, this stage is characterized by a slope lower in magnitude (if it is a negative slope) than the slopes of the regions represented by states A and C, or it can show a positive slope as shown in the inset. Hence, the friction stir processed alloy exhibited all three stages during work hardening. Each stage is a manifestation of a microscopic deformation process operative in the course of plastic deformation. Stages A and C are associated with the dislocation-slip-mediated plasticity. The stage B represents twinning-mediated plasticity, phase-transformation-induced plasticity, or a combination of both.

Work hardening is necessary for a material to undergo plastic deformation without the localized deformation. Stage A in Fig. 4c, d show a continuous drop in the strain hardening rate until stage B initiates. In the present case, stage B shows almost zero slope; therefore, it halts the drop of the strain-hardening rate. As mentioned, twinning- and transformation-induced plasticity have been attributed for such a change in the slope of the strain-hardening rate curve.¹⁷ The twin density has been observed to increase as deformation progresses in stage B.¹⁹ The balance of the strain-hardening rate and the rate of recovery determines the slope in

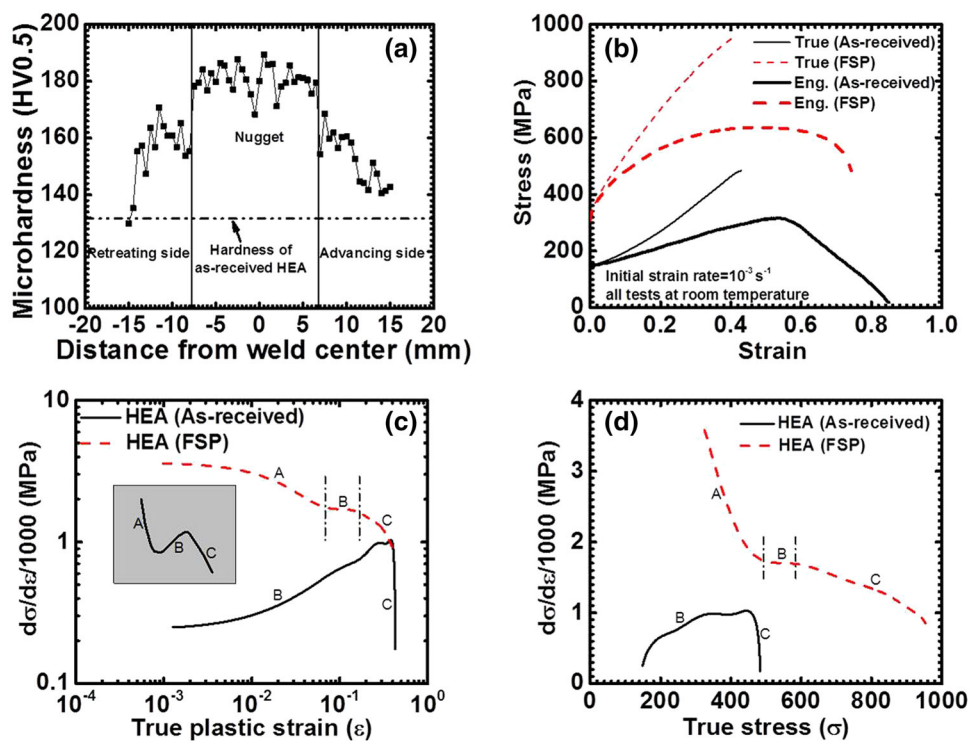


Fig. 4. (a) Microhardness distribution in the nugget on the transverse cross-section of the processed plate, (b) stress–strain curves, and (c) strain-hardening rate versus true strain plot. The schematic in the inset shows three stages of work-hardening rate¹⁷ and (d) strain-hardening rate versus true stress plot.

this stage. It is followed by stage C, which is similar to stage A. A microstructural investigation in each stage would be necessary to understand the actual deformation mechanism(s) operative in each stage.

Note that the friction stir processed alloy showed significant work-hardening ability during plastic deformation. In the true stress–true strain curves (Fig. 4b), the flow stress changed from 315 MPa to in excess of 900 MPa at the end of uniform plastic deformation, which represents a threefold increase in the flow stress. The result of such a high work-hardening rate is 50% uniform engineering strain (40% true strain). The total elongation shown was $\sim 75\%$ in this condition. Although the YS of the alloy in this condition is low, such a high level of total elongation suggests that this alloy can be subjected to further plastic deformation processes such as cold rolling to improve the strength of the alloy; this process will be akin to H temper used for conventional metallic alloys. In another work on the same alloy, in which a finer average grain size was obtained by FSP, showed yield strength of 544 MPa with a total elongation of $\sim 50\%$.⁹ Hence, a great potential exists for improving the strength of the alloy by further plastic deformation, grain refinement, or a combination of both while retaining an acceptable level of ductility.

Most of the mechanical properties reported for HEAs are based on hardness measurements and uniaxial compression tests. It is partly due to the

processing path used for HEAs. Conventional casting and powder metallurgy have been preferred routes so far in the manufacturing of HEAs. Casting- and sintering-related porosities render HEAs with almost no ductility.²⁰ The as-received alloy used in this study was subjected to the HIP process after casting, which aids in the elimination of casting porosities. Therefore, the alloy in the as-received condition exhibited very good ductility. Although FSP was applied in the HIP condition, in general, FSP can be applied to the as-cast condition, and it would result in a wrought microstructure in the processed zone. FSP causes a very good combination of strength and ductility in the processed zone as observed in this study, the YS of 315 MPa, uniform elongation of 50%, and total elongation of 75%; and in the previous study, the YS was 544 MPa, uniform elongation was $\sim 28\%$ and total elongation was $\sim 50\%$.⁹ In a recent study, it was shown that an HEA consisting of eutectic microstructure exhibited a very good work-hardening behavior that resulted in a fracture stress of 944 MPa with 23% total elongation. But it exhibited a very low level of YS (< 100 MPa) and sudden fracture of the tensile sample; i.e., there was no postnecking plastic deformation. Note that the current alloy in the FSP condition underwent $\sim 25\%$ postnecking deformation. Yao et al.²¹ reported that the single-phase fcc nonequiatomic FeMnNiCoCr HEA exhibited the YS of 240 MPa and total elongation $\sim 58\%$. In cold-rol-

led condition, the FeMnNiCoCr HEA demonstrated YS of 760 MPa and total elongation of $\sim 17\%$. These examples demonstrate a wide scope in the microstructural design by developing thermomechanical processing steps for HEA to obtain a wide range of mechanical properties for an array of structural applications.

Figure 5a plots the change in YS as a function of the average grain size. Mathematically, the contribution of grain-boundary strengthening is expressed by the Hall–Petch relationship, which is given as follows.

$$\Delta\sigma_{\text{HP}} = \sigma_0 + k_{\text{HP}}d^{-1/2} \quad (1)$$

where $\Delta\sigma_{\text{HP}}$, σ_0 , k_{HP} , and d are the grain-boundary strengthening contribution to YS, friction stress, Hall–Petch coefficient (also known as locking parameter), and average grain size, respectively. Equation 1 was fitted through three datum points present in Fig. 5a. For the as-received HEA, an average grain size of 2 mm ($2000 \mu\text{m}$) was chosen for the current analysis. Note that Figs. 2c and 3a indicate the presence of very large grains—in excess of $500 \mu\text{m}$. Hence, at such a large grain size, the grain-boundary contribution is almost negligible for fcc metals and alloys, and the contribution to the YS is mostly due to the friction stress in absence of other strengthening mechanisms.¹⁵ The second datum point corresponds to the average grain size and yield strength combination of the friction stir processed microstructure in the current study. The third datum point was taken from a recent work published by the current authors elsewhere.⁹ Note that for third datum point, the YS and average grain size were $544 \pm 27 \text{ MPa}$ and $0.95 \pm 0.31 \mu\text{m}$, respectively.⁹

Based on the linear regression analysis, σ_0 and k_{HP} were found to be 174 MPa and $371 \text{ MPa} (\mu\text{m})^{1/2}$, respectively. At this point, the friction stress σ_0 and Hall–Petch coefficients k_{HP} merit further discussion. The parameter k_{HP} from the current study is plotted in Fig. 5b along with many other fcc, body-centered cubic (bcc), and hexagonal close-packed

(hcp) metals and alloys.^{15,22–25} Figure 5b suggests that bcc and hcp metals and alloys have relatively higher k_{HP} than that of fcc materials. Based on the data related to fcc materials, k_{HP} values are less than $400 \text{ MPa} (\mu\text{m})^{1/2}$. As per this observation, the k_{HP} value determined for the $\text{Al}_{0.1}\text{CoCrFeNi}$ HEA investigated currently is impressive. Note that this value of k_{HP} is on the lower end of the k_{HP} values shown by bcc materials and at the higher end of fcc materials.

The normal stress (σ) and resolved shear stress (τ) are related by the following expression,

$$\sigma = M\tau \quad (2)$$

where M is the Taylor factor, which is taken as 3.1 for a randomly oriented cubic polycrystalline material.²⁶ Hence, dividing σ_0 by 3.1 gives the critical resolved shear stress (CRSS) of $\sim 56 \text{ MPa}$. Most of the pure fcc materials show CRSS values much smaller than the value observed for $\text{Al}_{0.1}\text{CrCoFeNi}$ alloy. With respect to hcp materials, the value of CRSS for the HEA is much higher, and it is at the lower end of the spectrum of CRSS values for bcc metallic materials.²²

Such a high value of the Hall–Petch coefficient has been noted by Liu et al.²⁷ in a recent study on a single-phase fcc FeCrNiCoMn alloy. In that study, Vickers microhardness values were plotted as a function of the inverse of the squared root of d . The slope was found to be equal to $677 \text{ MPa} (\mu\text{m})^{1/2}$ through the linear regression analysis. Such high values of the Hall–Petch coefficient for HEAs have been rationalized based on the complex dislocation core structure and its interaction with a very complex atomic potential well associated with lattice planes in HEAs.

SUMMARY AND CONCLUSION

A single-phase fcc $\text{Al}_{0.1}\text{CrCoFeNi}$ HEA consisted of considerably large grains in the as-received condition. FSP was used to refine the grain size of the alloy. The average grain size in the friction stir

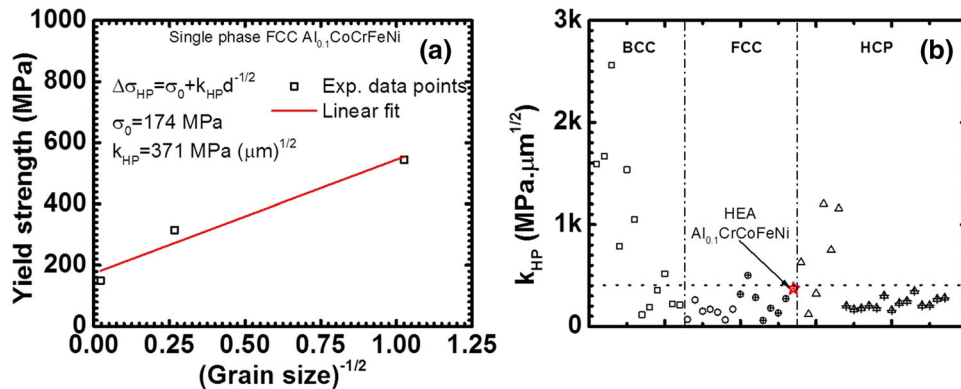


Fig. 5. (a) The variation of yield strength as a function of average grain size. (b) A comparison of the Hall–Petch coefficient (k_{HP}) of the $\text{Al}_{0.1}\text{CrCoFeNi}$ HEA with that published in literature for alloys with different crystal structures.^{15,22–24}

processed condition was $14 \pm 10 \mu\text{m}$. In the FSP condition, the HEA showed an excellent combination of strength and ductility; the total elongation of $\sim 75\%$ for the minitensile sample used and YS of 315 MPa. The Hall–Petch strengthening analysis showed the friction stress and the Hall–Petch coefficient to be 174 MPa and $371 \text{ MPa}(\mu\text{m})^{1/2}$, respectively. Such high values of friction stress and Hall–Petch coefficient indicate that grain refinement can be a very effective strengthening mechanism for this alloy.

REFERENCES

1. Y. Zhang, T.T. Zuo, Z. Tang, M.C. Gao, K.A. Dahmen, P.K. Liaw, and Z.P. Lu, *Prog. Mater. Sci.* 61, 1 (2014).
2. B. Cantor, *Entropy* 16, 4749 (2014).
3. J.-W. Yeh, S.-K. Chen, S.-J. Lin, J.-Y. Gan, T.-S. Chin, T.-T. Shun, C.-H. Tsau, and S.-Y. Chang, *Adv. Eng. Mater.* 6, 299 (2004).
4. D.B. Miracle, J.D. Miller, O.N. Senkov, C. Woodward, M.D. Uchic, and J. Tiley, *Entropy* 16, 494 (2014).
5. B. Gludovatz, A. Hohenwarter, D. Catoor, E.H. Chang, E.P. George, and R.O. Ritchie, *Science* 345, 1153 (2014).
6. O.N. Senkov, G.B. Wilks, J.M. Scott, and D.B. Miracle, *Intermetallics* 19, 698 (2011).
7. M.A. Hemphill, T. Yuan, G.Y. Wang, J.W. Yeh, C.W. Tsai, A. Chuang, and P.K. Liaw, *Acta Mater.* 60, 5723 (2012).
8. F. Otto, A. Dlouhý, C. Somsen, H. Bei, G. Eggeler, and E.P. George, *Acta Mater.* 61, 5743 (2013).
9. M. Komarasamy, N. Kumar, Z. Tang, R.S. Mishra, and P.K. Liaw, *Mater. Res. Lett.* 3, 30 (2015).
10. W.M. Thomas, E.D. Nicholas, J.C. Needham, M.G. Murch, P.T. Smith, and C.J. Dawes, U.S. patent WO1993010935 A1 (1993).
11. R.S. Mishra, M.W. Mahoney, S.X. McFadden, N.A. Mara, and A.K. Mukherjee, *Scripta Mater.* 42, 163 (1999).
12. R.S. Mishra, P.S. De, and N. Kumar, *Friction Stir Welding and Processing: Science and Engineering* (New York: Springer, 2014).
13. N. Kumar and R.S. Mishra, *Metall. Mater. Trans. A* 44, 934 (2013).
14. N. Kumar, M. Komarasamy, and R.S. Mishra, *J. Mater. Sci.* 49, 4202 (2014).
15. N. Kumar and R.S. Mishra, *Mater. Sci. Eng. A* 580, 175 (2013).
16. N. Kumar, D. Choudhuri, R. Banerjee, and R.S. Mishra, *Int. J. Plast* 68, 77 (2015).
17. A. Rohatgi, K. Vecchio, and G.T. Gray III, *Metall. Mater. Trans. A* 32, 135 (2001).
18. R.W.K. Honeycombe, *Plastic Deformation of Metals*, 2nd ed. (Maidenhead, UK: Edward Arnold Ltd., 1984).
19. R. Kapoor, A. Sarkar, J. Singh, I. Samajdar, and D. Raabe, *Scripta Mater.* 74, 72 (2014).
20. Y. Lu, Y. Dong, S. Guo, L. Jiang, H. Kang, T. Wang, B. Wen, Z. Wang, J. Jie, and Z. Cao, *Sci. Rep.* 4, Article# 6200 (2014).
21. M.J. Yao, K.G. Pradeep, C.C. Tasan, and D. Raabe, *Scripta Mater.* 72–73, 5 (2014).
22. D. Wu, J. Zhang, J.C. Huang, H. Bei, and T.G. Nieh, *Scripta Mater.* 68, 118 (2013).
23. W. Yuan, S.K. Panigrahi, J.-Q. Su, and R.S. Mishra, *Scripta Mater.* 65, 994 (2011).
24. K. Takeda, N. Nakada, T. Tsuchiyama, and S. Takaki, *ISIJ Int.* 48, 1122 (2008).
25. S. Rajasekhara, P. Ferreira, L. Karjalainen, and A. Kyröläinen, *Metall. Mater. Trans. A* 38, 1202 (2007).
26. G.E. Dieter, *Mechanical Metallurgy*, 3rd ed. (New York: McGraw-Hill Inc, 1986).
27. W.H. Liu, Y. Wu, J.Y. He, T.G. Nieh, and Z.P. Lu, *Scripta Mater.* 68, 526 (2013).